

Submitted to *INFORMS Journal on Data Science*

Low-Rank Robust Subspace Tensor Clustering for Metro Passenger Flow Modeling

Nurretin Dorukhan Sergin

School of Computing and Augmented Intelligence, Arizona State University, Tempe, AZ 85281

Jiuyun Hu

School of Computing and Augmented Intelligence, Arizona State University, Tempe, AZ 85281

Ziyue Li

Cologne Institute for Information Systems, University of Cologne, Cologne, Germany

EWI gGmbH, University of Cologne, Cologne, Germany, zlibn@wiso.uni-koeln.de

Chen Zhang

Department of Industrial Engineering, Tsinghua University, Beijing, China, zhangchen01@tsinghua.edu.cn

Fugee Tsung

Department of Industrial Engineering and Decision Analytics, Hong Kong University of Science and Technology, Hong Kong

Information Hub, Hong Kong University of Science and Technology (Guangzhou), China, season@ust.hk

Hao Yan

School of Computing and Augmented Intelligence, Arizona State University, Tempe, AZ 85281, haoyan@asu.edu

Abstract. Tensor clustering has become an important topic, specifically in spatiotemporal modeling, due to its ability to cluster spatial modes (e.g., stations or road segments) and temporal modes (e.g., time of the day or day of the week). Our motivating example is from subway passenger flow modeling, where similarities between stations are commonly found. However, the challenges lie in the innate high-dimensionality of tensors and also the potential existence of anomalies. This is because the three tasks, i.e., dimension reduction, clustering, and anomaly decomposition, are inter-correlated to each other, and treating them in a separate manner will render a suboptimal performance. Thus, in this work, we design a tensor-based subspace clustering and anomaly decomposition technique for **simultaneously** outlier-robust dimension reduction and clustering for high-dimensional tensors. To achieve this, a novel low-rank robust subspace clustering decomposition model is proposed by combining Tucker decomposition, sparse anomaly decomposition, and subspace clustering. An effective algorithm based on Block Coordinate Descent is proposed to update the parameters. Prudent experiments prove the effectiveness of the proposed framework via the simulation study, with a gain of **+25%** clustering accuracy than benchmark methods in a hard case. The interrelations of the three tasks are also analyzed via ablation studies, validating the interrelation assumption. Moreover, a case study in the station clustering based on real passenger flow data is conducted, with quite valuable insights discovered.

Key words: Subspace Clustering, Tensor Decomposition, Anomaly Detection, Spatiotemporal Analysis

History: This paper was first submitted on Oct 8th, 2022

1. Introduction

Higher-order tensors have been actively used in research since they have an inclination to successfully preserve the complicated correlation structures of data. A tensor can be defined mathematically as multi-

dimensional arrays (Kolda and Bader 2009). The order of a tensor is the number of dimensions, also known as modes. Tensor clustering is a recent generalization of the basic one-dimensional clustering problem to a high-dimensional version, and it seeks to partition an order- K input tensor into coherent sub-tensors (e.g., slices on one mode) while optimizing some cluster-related measuring criteria (Jegelka et al. 2009).

Tensor clustering has also become an important topic in spatiotemporal modeling (Sun and Li 2019, Bahadori et al. 2014, Mao et al. 2022), due to its ability to cluster complicated spatial modes (e.g., stations, road segments, etc.) and temporal modes (e.g., time of day or day of week). For example, in the modeling of passenger flow, similarities between spatial elements are commonly found in spatio-temporal data (Li et al. 2020a). These clusters may be due to natural geographical locations (e.g., neighboring stations) or contextual information (e.g., points of interest) in the context of where the data are collected. For example, in residential areas, stations often have a large number of in-flow passengers in the morning on weekdays; instead, in the business areas, in-flow peaks are expected in the afternoon on weekdays. Exploring metro station clusters can help public transportation management, like operational efficiency, Strategic Planning, Anomaly Detection, Policy Making, and Land Use Planning. Overall, the following two challenges present for data collected from such complex spatiotemporal systems.

1. **Complex spatio-temporal structure in high-dimensional data.** The dimensionality of the tensor data is often high (especially in the temporal domain), and traditional statistical methods may suffer from the “curse of dimensionality”. Furthermore, data points in the high-dimensional tensor often present complicated and high-order variations. For the temporal dependencies, passenger flow patterns show a strong periodicity with a period of 7 days, which denotes the weekly transit patterns (Li et al. 2020b). This can also be seen in Figure 1 (right). Furthermore, on the same day, there are also complicated dependencies. For example, there are often two in-flow peaks for the multi-functional regions in the daily profile during the weekdays, which represent the morning and afternoon time for the daily commute, whereas a dominant morning in-flow peak is usually observed in residential regions and an evening in-flow peak commonly in business regions. For spatial structures, we create a correlation heatmap of passenger flows in different stations on day 1, as shown in Figure 1 (left). Figure 1 (left) demonstrates two kinds of passenger flow similarities. The geographical similarity is based on the distance between the stations; while the contextual similarity is based on the function of the stations.

2. **Existence of sparse anomalies.** The tensor may contain sparse outliers due to measurement errors or rare events in urban passenger flow, such as weather, special occasions, etc. The sparse outliers may refer to the sudden increase of demand; this may be related to some unprecedented events happening, such as concerts and festivals, or this could even be due to maintenance or breakdowns in other stations whose spillover effect flows into the station in question. Identifying these events can also help prepare for the sudden increase in demand. To better understand the sparse anomaly feature, we create a correlation heatmap of passenger flows at station 1 on different days, as shown in Figure 1 (right). Figure 1 (right)

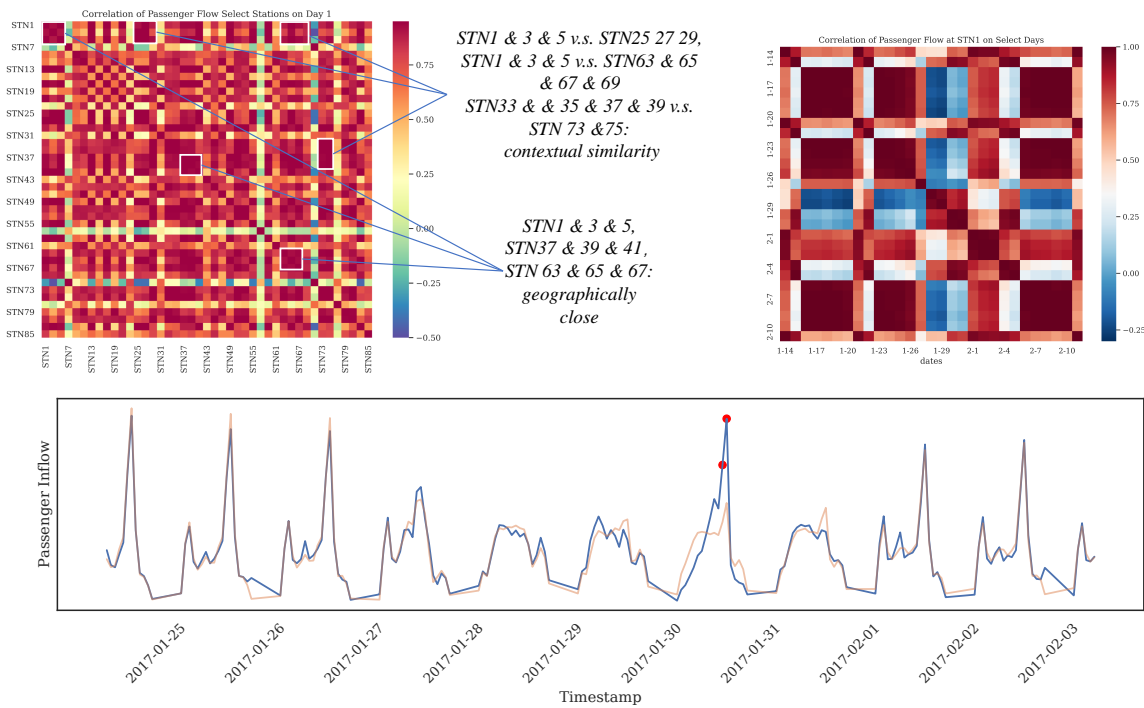


Figure 1 Correlation heatmaps showing (Left) geographical and contextual similarity between stations; (Right) temporal structure and sparse anomaly. (Bottom): Existence of sparse anomalies

shows that in most days, the passenger flow follows the temporal structure of the similarities of the weekday and weekend, except for 4 days. These days serve as the sparse anomaly in the data. Finally, to further illustrate the existence of "sparse anomalies", we have included another plot on the sparse anomalies, as shown in Figure 1 (bottom). A good example is illustrated here of an unexpected peak in the afternoon of January 30th, 2017, at the Fo Tan station. The peak is due to people leaving home from the Lunar New Year horse racing event, which takes place on the race course accessible from the Fo Tan station. Therefore, in this research, we define the "anomaly" study in this research as the entry-level pieces of the tensor data that do not fit the underlying distribution of the main features of the data.

In the literature, most of the methods implement a three-step approach for tensor clustering. First, tensor decomposition can be used to reduce the tensor dimensionality. Then, sparse outliers can be removed by robust tensor decomposition, and lastly, clusters can be identified by existing clustering algorithms such as K-Means or subspace clustering. In the first step of tensor decomposition, related to dimension reduction techniques, non-negative tensor decomposition (Lin et al. 2018), Tucker decomposition (Kolda and Bader 2009), and CP decomposition (Kolda and Bader 2009) are widely used. In the step of anomaly detection, to handle sparse outliers, Hu and Work (2021) proposed a robust tensor decomposition method that can handle outliers data while achieving dimension reduction. Unlike standard robust tensor decomposition applications, they used the $L_{2,1}$ norm as they assumed fiber-sparse anomalies. Finally, in the step of clustering,

it is quite common to apply clustering algorithms to the reduced-dimensional space. For example, Yang et al. (2019) proposed a hybrid approach that combines tensor decomposition with spectral clustering in a low-dimensional space.

However, none of these aforementioned works considers the interrelated nature of clustering, outlier removal, and dimension reduction (Aggarwal 2015), with the interrelation threefold as follows:

1. **Dimension Reduction and Clustering:** Clustering directly in the high dimensions will suffer from the “curse of dimensionality”, given that data becomes much more sparse and Euclidean distance is not a good distance measure in high-dimensional space. Therefore, dimension reduction techniques are often needed to project data in a low-dimensional space before clustering methods are applied (Yang et al. 2019).

2. **Outlier Decomposition and Clustering:** On the other hand, if outliers on stations are not correctly identified or decomposed, the results of clustering for the overall data from the normal patterns will also be compromised.

3. **Dimension Reduction and Outlier Decomposition:** Furthermore, a direct dimension reduction on the outliers-corrupted data will also lead to the introduction of erroneous information into the lower-dimensional products, i.e., decomposed latent matrices, which will hurt the downstream task performance (i.e., clustering) using the low-dimensional space.

In conclusion, we claim that the tensor clustering problem, dimension reduction, and outlier decomposition problem are inter-correlated tasks and tied to each other, and isolated treatment of them may fail to provide satisfactory performance.

In this paper, we propose a **Low-Rank Robust Tensor Subspace Decomposition (LRTSD)** technique to achieve dimensionality reduction, spatial clustering, and sparse anomaly decomposition *simultaneously*. The proposed method is inspired by the recent development in the following three fields: Tucker decomposition (Kolda and Bader 2009), tensor subspace clustering (Vidal 2011, Zhang et al. 2015), and sparse anomaly decomposition (Yan et al. 2017, Li et al. 2022a) (In this paper, we interchangeably use the term outlier and anomaly to represent the data which behaves outstandingly). Tucker decomposition is used as a dimensionality reduction technique, which reduces the original high-dimensional tensor data into a lower-dimensional core tensor while fitting orthonormal bases (Tucker 1966). Furthermore, the proposed method is inspired by the sparse anomaly decomposition methods (Yan et al. 2017, Li et al. 2022a), which aims to decompose the sparse anomaly component from the background component, with the L_1 norm applied to encourage the sparsity of detected anomalies. Finally, the proposed method is also inspired by the subspace clustering method (Vidal 2011), which has achieved especially good accuracy in high-dimensional clustering problems (Parsons et al. 2004).

In this paper, we innovatively apply subspace clustering to the core tensor in the Tucker Decomposition, which is inherently more resilient to corruption/anomaly. To our knowledge, this is the first instance of such integration, and our simulation studies substantiate its superior performance. The amalgamation of these

three components significantly increases the complexity of the model. To address this, we have developed an efficient optimization algorithm to overcome this challenge, ensuring the generalizability, computational feasibility, and enhanced accuracy of the tensor clustering model.

The remainder of this paper is organized as follows. Section 2 gives a brief overview of the basic tensor notations and multilinear algebra operation and subspace clustering. Section 3 provides a detailed introduction to the proposed subspace Tucker decomposition methods as well as an efficient optimization algorithm. Section 4 conducts a simulation study, and Section 5 apply the proposed method to a real dataset based on Hong Kong Metro data. Section 6 concludes and presents some future works.

2. Literature Review

In this section, we will briefly review the methodology related to tensor decomposition and subspace clustering methods for tensor data.

2.1. Tensor Decomposition

Related to robust tensor decomposition methods, most existing works apply the dimension reduction approach and tensor decomposition method for feature extraction.

Historically, all data is vectorized to the sample dimension, and the ordinary principal component analysis (PCA) is applied to the vectorized data to extract and monitor features, which is typically termed vectorized PCA (VPCA) (Nomikos and MacGregor 1994). However, such a method sacrifices the detection power, since the vectorization on high-dimensional data destroys the innate cross-dimensional relations.

Tensor is introduced as an efficient data structure to preserve inter-dimensional correlations well, such as complex spatiotemporal correlations among traffic data, as mentioned before. Tensor decomposition is developed accordingly to extract the features from the tensor data. Various tensor decomposition methods are developed, namely: (1) CANDECOMP/PARAFAC (CP) Decomposition (Hitchcock 1927), which represents a tensor $\mathcal{X} \in \mathbb{R}^{I_1 \times I_2 \times \dots \times I_K}$ as the weighted summation of a set of rank-one tensors; (2) Tucker Decomposition (Tucker 1966), which decomposes a tensor into a core tensor $\mathcal{C} \in \mathbb{R}^{J_1 \times J_2 \times \dots \times J_K}$ multiplied by a mode matrix $\mathbf{U}^{(k)} \in \mathbb{R}^{I_k \times J_k}$ along each dimension. The proposed method is based on the Tucker decomposition, and detailed operations of the Tucker decomposition will be introduced in Section 3.1.

Yan et al. (2015) proposed to utilize several anomaly detection and monitoring schemes based on Tucker Decomposition (Tucker 1966), Multi-linear PCA (Lu et al. 2008a), CP Decomposition (Hitchcock 1927), and Uncorrelated multi-linear PCA (Lu et al. 2008b) with the application for image-based anomaly detection. However, such approaches do not consider the properties of sparse outliers for anomaly detection. To address this problem, tensor-based sparse anomaly decomposition techniques have been proposed (Fanaee-T and Gama 2016) and applied into video-imaging data (Yan et al. 2018), urban traffic flow prediction (Sofuoglu and Aviyente 2021), crime rate monitoring (Zhao et al. 2021), pandemic monitoring (Zhao et al. 2020), etc. However, the major limitation of these existing tensor-based anomaly decomposition methods

is that they assume that the tensor follows a joint smooth and low-rank representation, which is not feasible for high-dimensional tensor data with multiple latent clusters behind the data distribution (Li et al. 2020a). However, a direct application of the decomposition method to the tensor data with outliers for clustering will render an oversimplified model.

2.2. Tensor Subspace Clustering

On the other hand, there are some recent literature focusing on clustering methods for tensor data. (Drakopoulos et al. 2019) gave an extensive methodology review of the tensor clustering. Some methods such as topic-model-based clustering (Li 2021, Li et al. 2022b), dynamic tensor clustering (Sun and Li 2019), multi-view subspace clustering (Zhang et al. 2015), dynamic subspace clustering (Zhang et al. 2020), joint K-means and high-order SVD (Huang et al. 2008) are proposed. Among them, subspace clustering has been a popular method for high-dimensional clustering (Parsons et al. 2004), which learns data representation in certain low-dimensional subspaces and clusters of the data points. The subspace clustering is commonly formulated based on the data's self-expression property (Gao et al. 2015), representing the original input data \mathbf{X} by itself: $\mathbf{X} = \mathbf{X}\mathbf{Z} + \mathbf{E}$, where $\mathbf{Z} \in \mathbb{R}^{n \times n}$ is the subspace representation matrix, and the nonzero elements in \mathbf{Z} correspond to the data points from the same subspace. Different properties could be achieved by introducing regularization terms into the representation matrix. More details will be explained in Section 3.2. However, like the other tensor clustering methods mentioned above, they are typically operated on the high-dimensional tensor directly and may suffer from the curse of dimensionality. For example, similar as tensor regression (Lock 2018, Gahrooei et al. 2021), directly applying self-expression on high-dimensional data leads to an even higher-dimensional self-expressiveness term.

Recently, there have been some works focusing on combining tensor low-rank decomposition and subspace clustering (Fu et al. 2014, 2016). Specifically, Fu et al. (2016) proposed a subspace clustering that incorporates sparse dictionary learning into tucker decomposition, where the tucker core tensor could be the input tensor itself (Fu et al. 2014) or the inverse matricization product of the dictionary and sparse representation (Fu et al. 2016). However, these subspace clustering methods are directly targeted at high-dimensional tensors, which are not suitable for tensors with sparse anomalies. Recently, there have been some efforts to combine subspace clustering methods with anomaly detection to handle the challenges of anomalies in multi-clustered datasets.

Recently, there have been a few developed tensor clustering methods based on deep learning and neural networks. (Wang et al. 2023) proposed the Tensorized Hypergraph Neural Networks (THNN) to learn the hypergraph structure on higher dimensions. In two-dimensional cases, further methods, such as spectral clustering, can be performed to cluster the nodes. However, this method only considered the hypergraph structure and did not take subspace learning and anomaly into consideration. (Zhao et al. 2022a) proposed the Reinforced Tensor Graph Neural Network (RTGNN) to learn multi-view graph data. This method

contains three modules, which makes it time-consuming. Tucker decomposition only takes part in the initialization, and the anomaly is neglected in this method. (Huang et al. 2023) extensively explored various methods, specifically on hyperspectral image clustering. The improvement achieved by neural network-based methods compared to tensor decomposition and self-regression-based methods is data-dependent. However, compared to the tensor-based approach, neural networks tend to become time-consuming and require many training samples.

2.3. Sparse Anomaly Decomposition

Anomaly is usually detected based on the assumption that anomalous data do not conform to expected behavior with outstandingly different features from the homogeneous background (Chandola et al. 2009). Traditional methods detect the anomaly based on distance and density, which assume that anomalies lie far away from the background or locate in a less dense area. Various definitions of distance or density have been introduced (Du and Zhang 2014). For example, (Sun et al. 2022) enhanced the CP decomposition by a deep CP decomposition neural network for feature extraction with an anomaly detection step. Nonetheless, to further achieve the separation of the anomalies, a further step such as clustering is still necessary. In this case, a one-step decomposition is favored in practice.

This paper is also motivated by the recent development of the decomposition-based methods (Sofuoglu and Aviyente 2021, Yan et al. 2017, Li et al. 2022a), which try to decompose the original input data into several components directly. For example, Yan et al. (2017) decomposed input data into the smooth background and sparse anomaly, with smoothness regularization on the background and sparsity penalty on the anomaly. Later, the extensions to spatiotemporal data (Yan et al. 2018), deep learning-based decomposition models (Zhao et al. 2022b) are proposed. For example, (Li et al. 2022a) considered more components, namely, smooth background, sparse anomaly, sample-specific deviation, and random noise, and they introduced a transfer learning mechanism (Pan and Yang 2009) to solve the cold-start problem for anomaly decomposition. However, these methods are not developed for tensor data, and the decomposed components are pre-defined in a fixed manner. Recently, Shen et al. (2022) proposed a tensor-based decomposition method to decompose the static tensor background and smooth foreground. However, the method is designed for static background and cannot be directly used to learn the tensor data from different subspaces. Our method instead is to combine the sparse decomposition method with the tensor decomposition approach, and it learns the hidden components in a data-driven and unsupervised manner via tensor subspace.

To summarize, this work is the first that achieves dimensionality reduction, spatial clustering, and anomaly decomposition simultaneously.

3. Methodology

In this section, we will first review the basic tensor algebra in Section 3.1. Then, we will give a brief review of the recent development of subspace clustering in Section 3.2. More specifically, we will discuss the

proposed formulation combining tensor subspace clustering in Section 3.3. We will then discuss how to solve the formulation efficiently in Section 3.4.

3.1. Basic Tensor Notation and Multilinear Algebra

In this section, we introduce basic notations, definitions, and operators in multilinear (tensor) algebra that is used in this work. Throughout the chapter, scalars are denoted by lowercase italic letters, e.g., a , vectors by lowercase boldface letters, e.g., \mathbf{a} , matrices by uppercase boldface letter, e.g., \mathbf{A} , and tensors by calligraphic letters, e.g., \mathcal{A} . For example, an order- K tensor is represented by $\mathcal{A} \in \mathbb{R}^{I_1 \times \dots \times I_K}$, where I_k represents the mode- k dimension of \mathcal{A} . The mode- k product of a tensor \mathcal{A} by a matrix $\mathbf{V} \in \mathbb{R}^{P_k \times I_k}$ is defined as follows:

$$(\mathcal{A} \times_k \mathbf{V})(i_1, \dots, i_{k-1}, j_k, i_{k+1}, \dots, i_K) = \sum_{i_k} A(i_1, \dots, i_k, \dots, i_K) V(j_k, i_k).$$

The Frobenius norm of a tensor \mathcal{A} can be defined as follows:

$$\|\mathcal{A}\|_F^2 = \sum_{i_1, \dots, i_K} A(i_1, \dots, i_k, \dots, i_K)^2.$$

The n -mode unfold operator maps the tensor \mathcal{A} into matrix $\mathbf{A}_{(n)}$, where the columns of $\mathbf{A}_{(n)}$ are the n -mode vectors of \mathcal{A} .

Tucker decomposition decomposes a tensor into a core tensor multiplied by a matrix along each mode, formulated as follows:

$$\mathcal{A} = \mathcal{C} \times_1 \mathbf{U}^{(1)} \times_2 \mathbf{U}^{(2)} \dots \times_K \mathbf{U}^{(K)},$$

where $\mathcal{C} \in \mathbb{R}^{J_1 \times J_2 \times \dots \times J_K}$ is the core tensor, $\mathbf{U}^{(k)}$ is an orthogonal $I_k \times J_k$ matrix and is a principal component mode- k . The definition of Kronecker product is as follows: Suppose $\mathbf{A} \in \mathbb{R}^{m \times n}$ and $\mathbf{B} \in \mathbb{R}^{p \times q}$ are matrices, the Kronecker product of these matrices, denoted by $\mathbf{A} \otimes \mathbf{B}$, is an $mp \times nq$ block matrix, which can be formalized as follows:

$$\mathbf{A} \otimes \mathbf{B} = \begin{bmatrix} a_{11}\mathbf{B} & \dots & a_{1n}\mathbf{B} \\ \vdots & \ddots & \vdots \\ a_{m1}\mathbf{B} & \dots & a_{mn}\mathbf{B} \end{bmatrix}$$

3.2. Subspace Clustering

An important but often unnoticed assumption of PCA is that the data lives in a *single* low-dimensional subspace. This assumption may be too crude for many applications, including spatiotemporal problems such as motion segmentation (Vidal et al. 2008). It is more likely in such cases that the data lives in a mixture of subspaces instead of a single one (see Figure 2). The field of subspace clustering deals with problems of this nature and has attracted growing interest in recent years (Liu et al. 2019, Guo et al. 2019).

The central problem of subspace clustering is the grouping of points and their respective clusters are both unknown in the beginning. Various frameworks have been proposed in recent years, ranging from direct

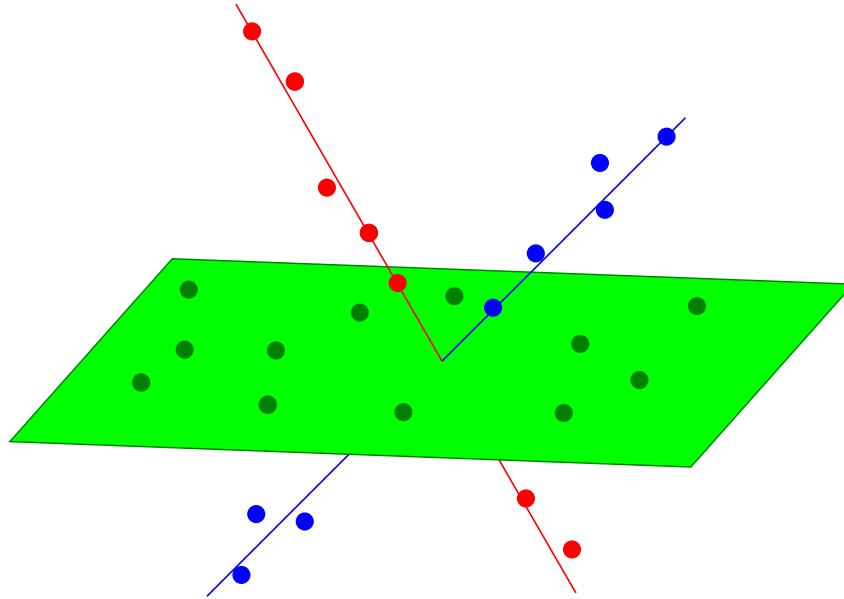


Figure 2 Data were drawn from two one-dimensional subspaces (red and blue) and one two-dimensional subspace (green). Adapted from (Vidal 2011).

algebraic solutions to probabilistic approaches (Vidal 2011), whereas spectral clustering (von Luxburg 2007) dominates the approaches proposed in recent years due to their superior performance over other frameworks. In short, spectral clustering aims to build a similarity graph where nodes are individual samples and the edges are similarity links. Algorithms such as graph cut can be used later to identify the clusters.

An effective way to obtain similarity is to use the self-expressiveness property (Parsons et al. 2004). Let $D \in \mathbb{R}^{n \times p}$ be a data matrix. The self-expressiveness can be defined with the equality $D = ZD$ where the self-expression matrix $Z \in \mathbb{R}^{n \times n}$ helps to express each point as a linear combination of other points in the data. This matrix can later be used to find clusters, as explained above.

Spectral subspace clustering methods differ in how they regulate the affinity matrix to avoid the trivial solution of identity matrix $Z = I$. Sparse subspace clustering (SSC) imposes sparsity on the affinity matrix (Yang et al. 2015), which is formulated as follows:

$$\min_Z \quad \|Z\|_1 + \frac{\lambda}{2} \|D - ZD\|_F^2 \quad s.t. \quad \text{diag}(Z) = 0,$$

where the $\|\cdot\|_1$ represent the L1 penalty of the self-expression matrix. By applying this penalty, the self-expression matrix Z is also assumed to be low-rank. Low-rank representation method was proposed by Liu et al. (2013). Similarly, another method of low-rank subspace clustering was developed by Vidal and Favaro (2014) where the core formulation uses the nuclear-norm of the self-expression matrix Z defined by the sum of its singular values as the best convex approximation of the rank of Z .

$$\min_{Z, D, A} \quad \|Z\|_* + \frac{\tau}{2} \|A - AZ\|_F^2 + \frac{\alpha}{2} \|D - A\|_F^2 \quad s.t. \quad Z^\top = Z$$

Thresholding ridge regression (TRR) (Peng et al. 2015) is an improvement on SSC in the sense that it relaxes the requirement to assume the structure of the affinity matrix, whether it is low-rank or sparse. The formulation is also much simpler.

$$\min_{\mathbf{Z}} \lambda \|\mathbf{Z}\|_F^2 + \|\mathbf{D} - \mathbf{DZ}\|_F^2$$

The regularization parameter λ represents the trade-off between the reconstruction fidelity and clustering ability, which may be set with respect to the use case. However, all these variations focus on the matrix formulation and cannot be applied to the tensor formulation.

3.3. Proposed Low-Rank Robust Tensor Subspace Decomposition (LRTSD) Model

Without loss of generality, we will illustrate the proposed method using a three-dimensional tensor. The methodology can be easily extended into higher-order tensors. For a three-dimensional tensor, we assume that $\mathcal{X} \in \mathbb{R}^{N \times I_2 \times I_3}$ to represent the original data, where the first dimension denotes the sample dimension that requires the clustering. Furthermore, we assume that this tensor \mathcal{X} can be decomposed into the normal variations data \mathcal{L} and the outlier tensor \mathcal{A} (i.e., represents anomalous inflows in the passenger flow data), which is assumed to be sparse. We assumed the normal variations data \mathcal{L} has a low-rank structure, which is a common assumption for high-dimensional tensors for dimension reductions. Furthermore, without loss of generality, we assume the first mode of tensor \mathcal{X} is the dimension that needs further clustering. We name the first mode of the tensor (mode 1) as the clustering mode and the other modes (modes 2 and 3) as the non-clustering modes.

For example, the passenger flow data can be represented as a tensor $\mathcal{X} \in \mathbb{R}^{N \times I_2 \times I_3}$, with the three modes representing the station (with N stations), the day of the week (with $I_2 = 7$ days), and the 5-minute time intervals (with $I_3 = 247$ intervals from 5 am to 1:30 am) within each day for the period where the subway station is open for, respectively. Each element of the tensor $X_{i,d,t}$ represents the inflow into stations i at day d and time interval t . Here, the station i is the clustering mode, and d and t are the non-clustering modes, given that the station s is often heterogeneous and may exhibit multiple clusters.

In this case, we propose to use a partial Tucker decomposition on the non-clustering modes as:

$$\mathcal{L} = \mathcal{C} \times_2 \mathbf{U}_2 \times_3 \mathbf{U}_3, \tag{1}$$

where a core tensor $\mathcal{C} \in \mathbb{R}^{N \times P_2 \times P_3}$ reduces the dimensionality of the original tensor. \mathbf{U}_2 and \mathbf{U}_3 are respective orthogonal matrices for the non-clustering modes. We propose to find subspaces in the latent space on the core tensor \mathcal{C} as opposed to original space, as this is computationally more efficient. Here, the notations that will be used in the paper are given in Table 1.

Using the thresholding ridge regression framework (Peng et al. 2015), we utilize the self-expressive expression $\mathcal{C} - \mathcal{C} \times_1 \mathbf{Z}$ by regularizing the self-expression matrix $\mathbf{Z} \in \mathbb{R}^{N \times N}$ using Frobenius norm. Formally, the model is described as an optimization problem:

Table 1 Notations for Proposed LRTSD Model.

Notation	Explanation
$\mathcal{X} \in \mathbb{R}^{N \times I_2 \times I_3}$	N : number of samples, I_2, I_3 : feature dimensions
$\mathcal{C} \in \mathbb{R}^{N \times P_2 \times P_3}$	Core tensor, with reduced dimensions P_2, P_3
$\mathbf{U}_l \in \mathbb{R}^{I_l \times P_l}, l = 2, 3$	orthogonal matrices for dimension reduction
$\mathcal{A} \in \mathbb{R}^{N \times I_2 \times I_3}$	Anomaly tensor, same size as \mathcal{X}
$\mathbf{Z} \in \mathbb{R}^{N \times N}$	Self-expression matrix

$$\min_{\mathbf{Z}, \mathcal{C}, \mathbf{U}_2, \mathbf{U}_3, \mathcal{A}} \frac{1}{2} \|\mathbf{Z}\|_F^2 + \frac{\lambda_z}{2} \|\mathcal{C} - \mathcal{C} \times_1 \mathbf{Z}\|_F^2 + \lambda_a \|\mathcal{A}\|_1 + \frac{\lambda_e}{2} \|\mathcal{X} - \mathcal{A} - \mathcal{C} \times_2 \mathbf{U}_2 \times_3 \mathbf{U}_3\|_F^2 \quad (2)$$

$$\mathbf{U}_2^\top \mathbf{U}_2 = \mathbf{I} \quad (3)$$

$$\mathbf{U}_3^\top \mathbf{U}_3 = \mathbf{I} \quad (4)$$

In summary, each term in the Equation (2) achieves following purpose:

- $\|\mathcal{X} - \mathcal{A} - \mathcal{C} \times_2 \mathbf{U}_2 \times_3 \mathbf{U}_3\|_F^2$ is the error term between the original input data \mathcal{X} and the two decomposed components, i.e., anomaly \mathcal{A} and low rank structure $\mathcal{L} = \mathcal{C} \times_2 \mathbf{U}_2 \times_3 \mathbf{U}_3$;
- $\|\mathcal{C} - \mathcal{C} \times_1 \mathbf{Z}\|_F^2$ is the self-expression term in tensor subspace clustering and is imposed on the decomposed core tensor. $\|\mathbf{Z}\|_F^2$ is the ridge regularization;
- $\|\mathcal{A}\|_1$ is the sparsity regularization term for the anomaly.

To this end, this model achieves what we promised “a simultaneous framework for dimension reduction, spatial clustering, and anomaly detection”.

3.4. Optimization Procedure

In this section, we propose an efficient algorithm to solve the proposed optimization problem Equation (2) - Equation (4). We will utilize the Block Coordinate Descent procedure to obtain each one of the model parameters blocks $\mathbf{Z}, \mathcal{C}, \mathbf{U}_2, \mathbf{U}_3$ and \mathcal{A} iteratively while keeping the others fixed from the last iteration. When Algorithm 1 terminates through convergence, graph cut is applied to $\mathbf{L} = \mathbf{Z}^\top + \mathbf{Z}$ to achieve clusters, and \mathcal{A} can be analyzed for detected point anomalies. The rationale of the proofs of the propositions are relegated to the Appendix.

3.4.1. Calculating the Self-expression Matrix The subproblem for optimizing \mathbf{Z} when all other parameters are fixed is

$$\min_{\mathbf{Z}} \frac{1}{2} \|\mathbf{Z}\|_F^2 + \frac{\lambda_z}{2} \|\mathbf{C}_{(1)} - \mathbf{Z}\mathbf{C}_{(1)}\|_F^2 \quad (5)$$

Algorithm 1: Low-rank and Sparse Tensor Decomposition with Ridge Regularized Subspace Clustering

Data: \mathcal{X}, N, P_2, P_3

Result: $\mathcal{A}, \mathcal{C}, \mathbf{U}_2, \mathbf{U}_3, \mathbf{Z}$

Initialize $\mathcal{A} = \mathbf{0}, \mathbf{Z} = \mathbf{I}$. Initialize $\mathcal{C}, \mathbf{U}_2, \mathbf{U}_3$ by applying Tucker decomposition on \mathcal{X} ;

while *not converged* **do**

 Update \mathbf{Z} as in Equation (6) ;

 Update \mathcal{A} as in Equation (8) ;

 Update \mathcal{C} as in Equation (10) ;

 Update \mathbf{U}_2 and \mathbf{U}_3 as in Equation (12) ;

end

PROPOSITION 1. *The optimization problem in Equation (5) admits a closed-form solution,*

$$\mathbf{Z}^* = \lambda_z (\mathbf{I} + \lambda_z \mathbf{C}_{(1)} \mathbf{C}_{(1)}^\top)^{-1} (\mathbf{C}_{(1)} \mathbf{C}_{(1)}^\top) \quad (6)$$

Equation (5) suggests that there are only two terms in the problem related to the self expression matrix \mathbf{Z} . Proposition 1 derived a closed-form solution.

3.4.2. Calculating the Sparse Anomaly Tensor The subproblem for optimizing \mathcal{A} when all other parameters are fixed is

$$\min_{\mathcal{A}} \lambda_a \|\mathcal{A}\|_1 + \frac{\lambda_e}{2} \|\mathcal{X} - \mathcal{A} - \mathcal{C} \times_2 \mathbf{U}_2 \times_3 \mathbf{U}_3\|_F^2 \quad (7)$$

PROPOSITION 2. *The optimization problem in Equation (7) admits a closed-form solution using the soft-thresholding operator,*

$$\mathcal{A}^* = \text{sgn}(\mathcal{X} - \mathcal{C} \times_2 \mathbf{U}_2 \times_3 \mathbf{U}_3) \odot \max(\mathbf{0}, |\mathcal{X} - \mathcal{C} \times_2 \mathbf{U}_2 \times_3 \mathbf{U}_3| - \frac{\lambda_a}{\lambda_e}) \quad (8)$$

The proof follows directly on using soft thresholding in solving the orthogonal LASSO problem and is therefore omitted here.

3.4.3. Calculating the Core Tensor The subproblem for optimizing \mathcal{C} is

$$\min_{\mathcal{C}} \frac{\lambda_z}{2} \|\mathcal{C} - \mathcal{C} \times_1 \mathbf{Z}\|_F^2 + \frac{\lambda_e}{2} \|\mathcal{X} - \mathcal{A} - \mathcal{C} \times_2 \mathbf{U}_2 \times_3 \mathbf{U}_3\|_F^2 \quad (9)$$

PROPOSITION 3. *Define $\mathbf{M} \triangleq \mathbf{X}_{(1)} - \mathbf{A}_{(1)}$ and $\mathbf{P} \triangleq (\mathbf{U}_3 \otimes \mathbf{U}_2)^\top$. The optimization problem in Equation (9) admits a closed-form solution*

$$\mathbf{C}_{(1)}^* = \lambda_e (\lambda_z (\mathbf{I} - \mathbf{Z})^\top (\mathbf{I} - \mathbf{Z}) + \lambda_e \mathbf{I})^{-1} \mathbf{M} \mathbf{P}^\top \quad (10)$$

The resulting matrix $\mathbf{C}_{(1)}^*$ is folded back to the original tensor \mathcal{C} after the calculation.

3.4.4. Calculating the Orthonormal Bases When all other parameters are fixed, the subproblem to update U_2 is

$$\begin{aligned} \min_{U_2} \frac{\lambda_e}{2} \| \mathcal{X} - \mathcal{A} - \mathcal{C} \times_2 U_2 \times_3 U_3 \|_F^2 \\ U_2^\top U_2 = I \end{aligned} \quad (11)$$

PROPOSITION 4. Define $Q \triangleq (\mathbf{X}_{(2)} - \mathbf{A}_{(2)})(U_3 \otimes I)C_{(2)}^\top$ and let $Q = \hat{U}D\hat{V}^\top$ be the singular value decomposition of Q . Thus, the optimization problem in Equation (11) admits a closed-form solution for the optimal values for the first orthogonal basis U_2^*

$$U_2^* = \hat{U}\hat{V}^\top \quad (12)$$

Finally, the update of U_3^* is similar, therefore, omitted. In conclusion, the update of U_2^* and U_3^* both yield closed-form solutions.

4. Simulation Study & Results

In this section, we will evaluate the proposed methods via a simulation study. We will first introduce the simulation setup in Section 4.1. Then, the proposed method will be evaluated and compared with several clustering-based benchmark methods in Section 4.3.

4.1. Simulation Setup

In this section, we formalize the simulation procedure we use to generate clustered 3-order tensors with dimensionality $N \times I_2 \times I_3$. First, the procedure calls for the parameters in Table 2. After defining these parameters and setting the random number generating seed, we follow the following procedure to generate the data:

- For each cluster k and mode of tensor $l = 2, 3$, generate random factor matrices $U_{k,l} \in \mathbb{R}^{I_l \times P_l}$ from standard normal distribution, then orthogonalize $U_{k,l}$ via the QR decomposition.
- For each cluster k , generate a random core tensor $C_k \in \mathbb{R}^{N \times P_2 \times P_3}$ from standard normal distributions.
- For each cluster k , generate $\mathcal{X}_k = C_k \times_2 U_{k1} \times_3 U_{k2} + \epsilon$, where noise is added on each element of \mathcal{X} as $\epsilon \sim \mathcal{N}(0, \sigma^2)$, with $\sigma^2 = 0.25$.
- Elementwise add sparse anomaly $\mathcal{X} \leftarrow \mathcal{X} + \psi \mathcal{A}_p$. Each entry of \mathcal{A}_p is generated from the Bernoulli distribution with probability. Here p is the anomaly ratio. In each entry where \mathcal{A}_p is 1, indicating anomaly is present, we add the anomaly intensity constant ψ to the data.

Figure 3 provides a visual representation of the simulation data generation process. This procedure allows us to control key elements of the data generating process, such as the number of clusters, the cluster dimensions, the prevalence of anomalies, and how gross the anomalies are. We will now experiment with these factors and their effect on how well our model clusters samples and/or detects anomalies.

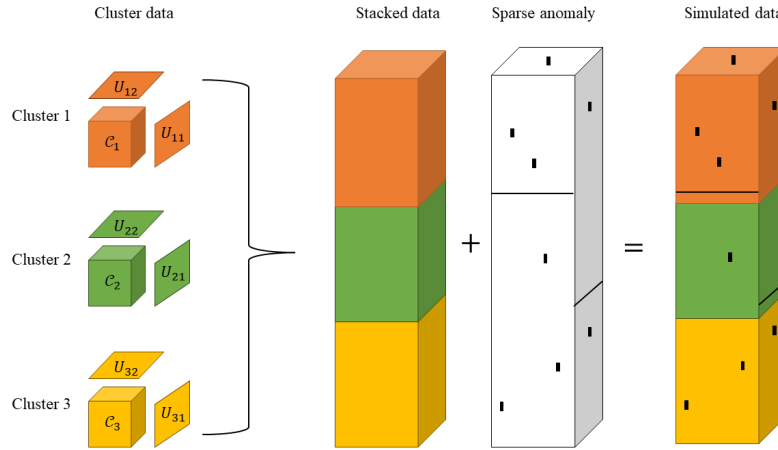


Figure 3 Illustration depicting the generation process of simulated data

Table 2 Required parameters for simulated clustered data generation and their notation.

Notation	Explanation
$K \in \mathbb{Z}^+$	Number of clusters
$N \in \mathbb{Z}^+$	Number of samples per cluster
$D_l \in \mathbb{Z}^+$	Ambient dimension of l^{th} mode
$P_l \in \mathbb{Z}^+$	Intrinsic dimension of l^{th} mode
$\sigma \in \mathbb{R}^+$	Standard deviation of random noise
$\mathcal{A}_p \in \mathbb{B}^{D_1 \times \dots \times D_L}$	Sparse anomaly index tensor with $0 < p < 1$ of entries being 1 and others 0
$\psi \in \mathbb{R}$	Sparse anomaly intensity

4.2. Tuning Parameters Selection

The proposed LRTSD has three tuning parameters: λ_e penalizes the norm of the self-regression matrix; λ_z penalizes the self-regression error of the core tensor; λ_a penalizes the norm of the anomaly tensor. These three tuning parameters are in comparison to the reconstruction error term, which has a coefficient of 1.

Related to the anomaly tuning parameter λ_a , one can select based on the percentage of nonzero anomaly entries expected in the dataset. For example, we can select the anomaly entries as a fixed percentage if we have some rough ideas on the percentage of the anomaly entries. If such a percentage is unknown, Otsu's method can be used to automatically select the tuning parameter λ_a , which aims to search for λ_a that minimizes the intra-class variance, defined as a weighted sum of variances of the two classes: normal class and abnormal class. This procedure is discussed in detail in (Yan et al. 2017). To select other tuning parameters, such as λ_e and λ_z , we propose using the normalized cut score. For λ_e and λ_z , λ_e yields smaller diagonal values in the self-regression matrix \mathbf{Z} ; higher λ_z yields a more precise self-regression. To address the challenge of unknown clustering accuracy, we propose using the normalized cut to evaluate the affinity matrix produced by the algorithm (Zhang et al. 2023) and select the tuning parameters λ_e and λ_z that produce the most reasonable affinity matrix by minimizing the normalized cut score. This measurement is

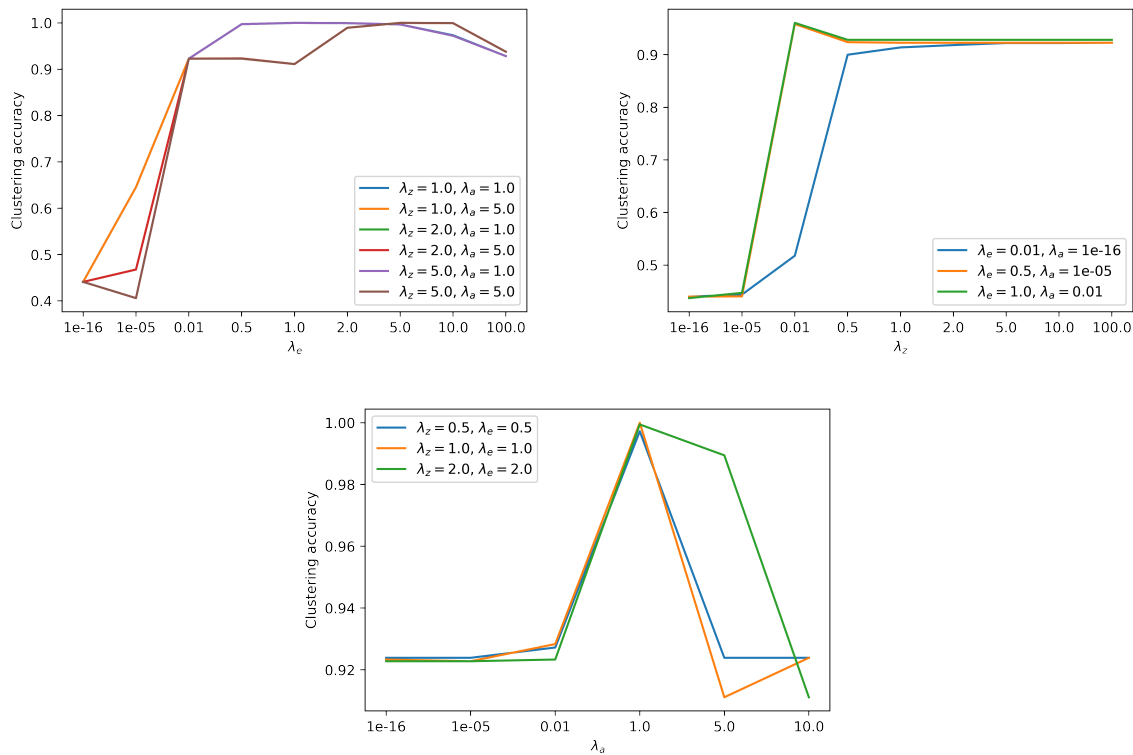


Figure 4 Clustering Accuracy of Different Tuning Parameter Combinations

defined by $NC = \sum_{c=1}^C \frac{W_c^{out}}{W_c^{in} + W_c^{out}}$, where c is the index of the cluster and W_c^{in} and W_c^{out} are the sum of the weights of the graph within the cluster and the weights of the graph outside the cluster. Smaller NC means better clustering.

Some examples of clustering accuracy for different combinations of tuning parameters are shown in Figure 4. From Figure 4, we can see that (1) λ_e , λ_z , λ_a cannot be too small, since we will almost lose a penalty term when any of the parameters are too small, which affects the clustering accuracy. (2) As λ_e and λ_z increase, the clustering precision increases. When λ_e continues to increase, the clustering accuracy will decrease because the corresponding terms will dominate optimization. (3) λ_a cannot be too small or too big, because we will not penalize the anomaly term when it is too small, and it will be too hard to discover any anomaly when λ_a is too big.

4.3. Performance Evaluation and Comparison

We generate a simulated three-dimensional tensor with three groups, thirty samples per cluster, fifty as the ambient dimensionality of each mode, and five as the intrinsic dimension on each mode. Therefore, the dimensionality of the data tensor is $90 \times 50 \times 50$. This can be considered representative of a spatio-temporal observation with one spatial dimension and two temporal dimensions with the inherent clustered structure and redundant information with respect to dimensionality. In this section, we compare the clustering accuracy of our models and three benchmark models under different anomaly ratios, and anomaly intensity,

where anomaly ratios are defined as the ratio of anomaly entry compared to the entire tensor dimensions and anomaly intensity denotes ψ . The clustering accuracy is defined by the maximum proportion of matching labels of the 90 objects in the first dimension over all permutations of the labels. The benchmark methods we compared are introduced below:

- **K-means**: For each of the 90 objects, we reshape the two-dimensional 50×50 matrix to a vector of length 2500. We make 3 groups using K-means based on the Euclidean distance.
- **Robust Tucker+K means**: We first use the Robust Tucker decomposition introduced in (Heng et al. 2023, Xue et al. 2017) to reduce the dimension to 15×15 for each object. We then use K means to generate 3 clusters based on the vectorized core tensor.
- **Multi-mode Tensor Space Clustering** (He and Atia 2022): This is a method based on low-rank tensor representation (LTRR). We will use single-mode tensor space clustering for two reasons. Firstly, all the other methods use a single mode, and thus it makes for a fair comparison. Secondly, when we increased the number of modes, the running time increased dramatically.
- **Robust Subspace Clustering** (Peng et al. 2015): This method is based on the thresholding ridge regression (TRR) and is compatible with the matrix data. Therefore, we first reshaped the $90 \times 50 \times 50$ tensor into the 90×2500 matrix and made 3 clusters.

When comparing the performance of LRTSD and the benchmark methods, we use a grid search of the tuning parameters and report the best clustering precision in different settings, namely $\lambda_e, \lambda_c, \lambda_a$ in LRTSD, representation rank r in LTRR, balance and thresholding parameter λ and k in TRR. We report the mean accuracy of 20 replications of data generation and clustering accuracy for each anomaly ratio & anomaly intensity combination and each method. The clustering accuracy result is shown in Table 3 with their standard deviation over the 20 replications in parentheses. In each combination of anomaly intensity and anomaly ratio, the best clustering accuracy is highlighted in bold. From the clustering accuracy result, we can see that the K-means and Robust Tucker + K means methods yield the two lowest accuracy proportion. This is because they are not designed specifically for clustering, and suffer from the curse of dimensionality when vectorized. When the anomaly ratio and intensity are not large, LRTSD, TRR, and LTRR have almost perfect clustering accuracy. As the intensity and ratio of the anomalies increase, the LTRR and TRR start to show errors. The threshold at which the two methods start to have incorrect clustering labels is smaller than that of LRTSD. Meanwhile, although LRTSD achieves the highest clustering accuracy, it does not require much more time compared to benchmark methods. The average processing times for K-means, Robust Tucker + K means, LTRR, TRR, and LRTSD are 0.06 second, 0.68 second, 0.08 second, 0.51 second, 0.71 second, respectively.

4.4. Sensitivity Analysis

More specifically, we aim to answer two major questions by comparing the proposed methods with several benchmark methods in terms of anomaly detection accuracy and clustering accuracy.

Table 3 Clustering accuracy for LRTSD and other three benchmarks

Ratio		0.05	0.1	0.125	0.15	0.175	0.2	0.225
Intensity	Method							
4	K mean	0.49 (0.02)	0.45 (0.03)	0.45 (0.03)	0.47 (0.02)	0.47 (0.02)	0.45 (0.02)	0.45 (0.03)
	Robust Tucker+K means	0.5 (0.03)	0.5 (0.03)	0.49 (0.03)	0.45 (0.02)	0.48 (0.02)	0.47 (0.02)	0.45 (0.02)
	LTRR	1 (0)						
	TRR	1 (0)	1 (0)	1 (0)	0.99 (0.01)	0.98 (0.01)	0.97 (0.01)	0.97 (0.01)
	LRTSD	1 (0)						
5	K mean	0.47 (0.02)	0.44 (0.02)	0.46 (0.03)	0.44 (0.03)	0.46 (0.03)	0.44 (0.03)	0.44 (0.03)
	Robust Tucker+K means	0.47 (0.03)	0.47 (0.03)	0.48 (0.02)	0.45 (0.03)	0.43 (0.03)	0.43 (0.03)	0.43 (0.02)
	LTRR	1 (0)	1 (0)	1 (0)	1 (0)	0.99 (0.01)	0.98 (0.01)	0.97 (0.02)
	TRR	0.99 (0.01)	0.99 (0.01)	0.98 (0.01)	0.96 (0.02)	0.99 (0.01)	0.96 (0.02)	0.98 (0.01)
	LRTSD	1 (0)						
6	K mean	0.44 (0.02)	0.44 (0.02)	0.43 (0.03)	0.44 (0.03)	0.43 (0.03)	0.42 (0.04)	0.42 (0.03)
	Robust Tucker+K means	0.46 (0.03)	0.46 (0.02)	0.45 (0.04)	0.43 (0.02)	0.41 (0.02)	0.41 (0.03)	0.4 (0.02)
	LTRR	1 (0)	1 (0)	0.99 (0.01)	0.99 (0.01)	0.96 (0.02)	0.94 (0.02)	0.87 (0.05)
	TRR	0.99 (0.01)	0.96 (0.02)	0.97 (0.02)	0.96 (0.02)	0.9 (0.04)	0.87 (0.05)	0.81 (0.05)
	LRTSD	1 (0)						
7	K mean	0.44 (0.02)	0.41 (0.03)	0.4 (0.03)	0.41 (0.03)	0.4 (0.04)	0.39 (0.03)	0.41 (0.03)
	Robust Tucker+K means	0.45 (0.04)	0.43 (0.03)	0.43 (0.03)	0.4 (0.04)	0.39 (0.02)	0.4 (0.03)	0.39 (0.02)
	LTRR	1 (0)	0.99 (0.01)	0.98 (0.01)	0.96 (0.02)	0.83 (0.07)	0.74 (0.09)	0.64 (0.12)
	TRR	0.97 (0.01)	0.94 (0.02)	0.9 (0.04)	0.79 (0.1)	0.76 (0.09)	0.64 (0.11)	0.63 (0.08)
	LRTSD	1 (0)						
8	K mean	0.44 (0.02)	0.39 (0.02)	0.39 (0.03)	0.4 (0.02)	0.39 (0.03)	0.41 (0.03)	0.4 (0.03)
	Robust Tucker+K means	0.42 (0.03)	0.41 (0.04)	0.41 (0.03)	0.4 (0.03)	0.4 (0.02)	0.39 (0.02)	0.39 (0.03)
	LTRR	1 (0)	0.94 (0.01)	0.86 (0.04)	0.74 (0.07)	0.58 (0.09)	0.54 (0.08)	0.53 (0.08)
	TRR	0.98 (0.01)	0.86 (0.05)	0.82 (0.08)	0.78 (0.11)	0.74 (0.09)	0.51 (0.06)	0.47 (0.07)
	LRTSD	1 (0)	1 (0)	1 (0)	1 (0)	1 (0)	1 (0)	0.99 (0.01)

- Question 1: *If sparse and gross anomalies are present, does anomaly detection lead to better clustering?*
- Question 2: *Does the tensor decomposition and dimension reduction lead to better clustering?*

4.4.1. The Effect of Dimensionality Reduction on Clustering Accuracy We generate a simulated three-dimensional tensor with three clusters, thirty samples per cluster, and 125 as the data dimensionality on each mode, namely, $90 \times 125 \times 125$, where the intrinsic dimensionality is 5 in each cluster. Therefore, the total intrinsic dimensionality of the tensor is actually $5 \times 3 = 15$. This can be considered representative of a spatiotemporal observation with one spatial dimension and two temporal dimensions with the inherent clustered structure and redundant information with respect to dimensionality.

For each seed, we generate some data and apply dimensionality reduction by a certain factor on each mode. The dimension reduction factor $\rho_d = [(\prod_l I_l / P_l)^{1/l}]$ is defined as the geometric mean of the data dimensionality I_l over the intrinsic dimension P_l averaged on different mode l of the tensor. For one factor of the experiment, we do not apply any dimensionality reduction (which is denoted by a factor of 1 on the x -axis in Figure 5). In other words, we directly apply subspace clustering on the high-dimensional tensor, optimizing the following objective:

$$\min_{\mathbf{Z}} \lambda \|\mathbf{Z}\|_F^2 + \|\mathbf{X}_1 - \mathbf{X}_1 \mathbf{Z}\|_F^2$$

Figure 5 shows the result of difference from minimum accuracy. For each replication, we obtain the clustering accuracy for different dimensionality reduction factors. Then they are subtracted from the minimum clustering accuracy within that replication and get the difference for each dimensionality reduction factor. After 20 replications, we get the result of 20 accuracy differences for each dimensionality reduction factor. Their mean is plotted in Figure 5. Observing Figure 5, there is an optimal range of dimensionality reduction ratio around 8 to 10, which roughly corresponds to the true intrinsic dimension ratio, i.e., $125/15 = 8.33$. This clearly suggests that clustering is more effective at the right proportion of dimensionality reduction, supporting our claim that dimension reduction improves the tensor clustering performance.

4.4.2. The Effect of Anomaly Detection on Clustering Performance The parameters for generating the simulation data are set to be the same as those in Section 4.3.

We factorize our experiment over the properties of the added sparse anomaly. Specifically, we alter how prevalent the anomaly is and how large its intensity is. At each factor of the experiment, we define the control group as the absence of anomaly detection, in other words, removing the term $\frac{\lambda_a}{2} \|\mathcal{A}\|_1$ from Equation (2). The treatment group is Equation (2) as is; therefore, the algorithm tries to detect the sparse anomaly. We do this over multiple seeds, where in each seed the exact same observations are used for both the control and treatment groups. We report the difference in clustering accuracy between the treatment group and the control group to identify whether anomaly detection would increase clustering accuracy or not. The

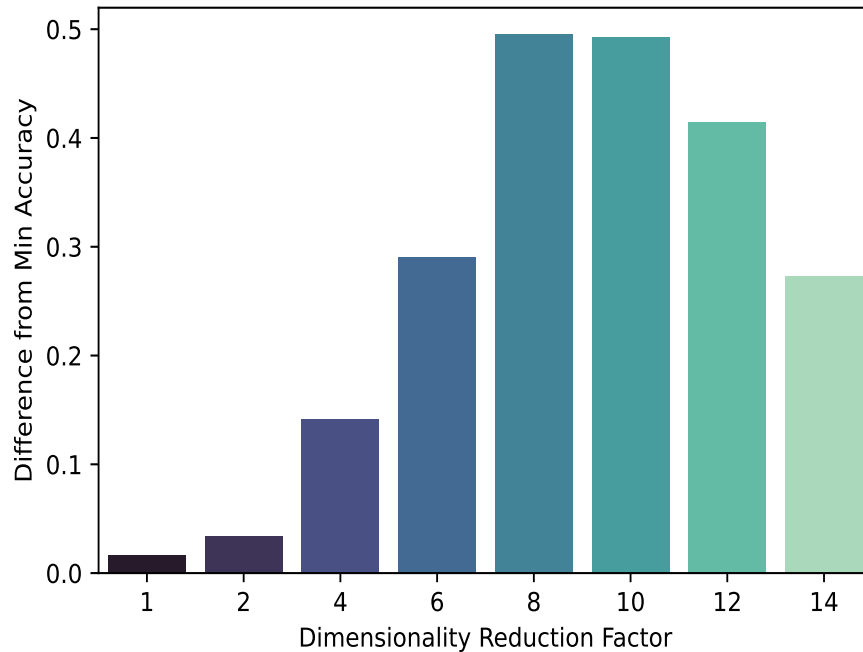


Figure 5 The evolution of clustering accuracy over multiple replications by increasing dimensionality factor on each mode.

clustering accuracy is defined as almost the same as the well-known clustering accuracy, except that the permutation of the labels is allowed such that it maximizes the agreement between the predicted labels and the ground truth.

In Figure 6, we observe a clear relationship between the severity of the anomalies and how much anomaly detection improves clustering performance. As the intensity of the anomaly increases and/or the prevalence of anomalies increases, the application of anomaly detection becomes even more significant in terms of finding the right groupings between the samples of the data. This can be considered quite an expected finding, but it is an important sanity check of our optimization procedure, and it finalizes the discussion of why simultaneous anomaly detection is crucial for the quality of cluster discovery.

5. Case Study & Results

We apply our proposed methodology to the smart card data collected by MTR, the company that operates Hong Kong’s subway system. Smart card data emerged as an important ingredient for urban mobility analysis, as it can be collected cheaply and contains detailed information about how people move within a city (Pelletier et al. 2011). Using this information, decisions at the tactical or strategic level can be made in a data-driven, thus more effective manner.

The data span an 82-day time horizon from January 1st 2017 and record every tap-in and tap-out event from 85 stations of the system. We resample these events hourly for each day within the operating hours

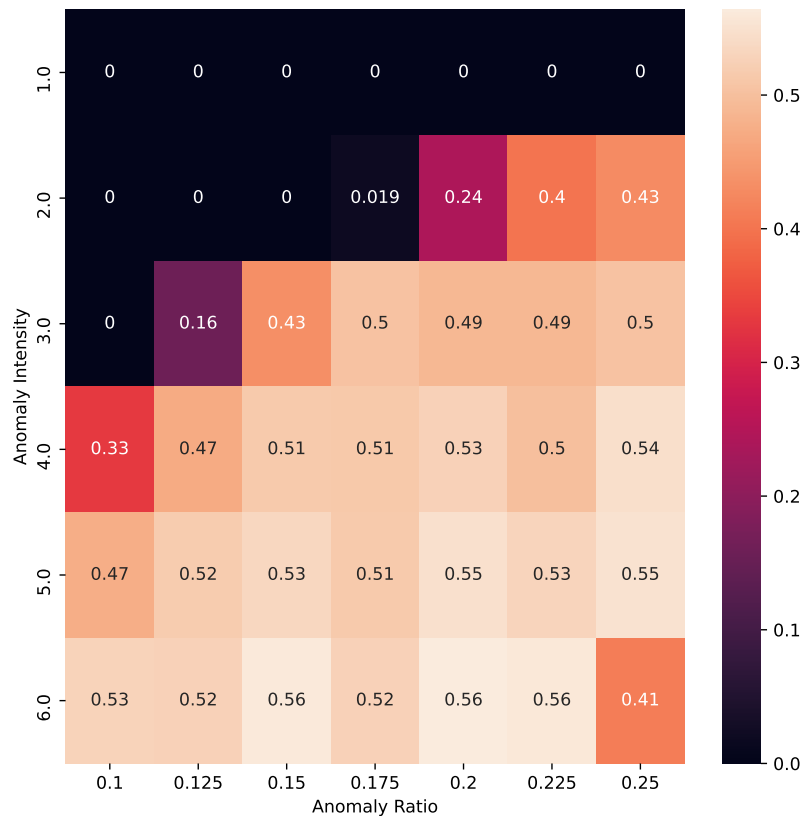


Figure 6 The average of pairwise differences in clustering accuracy between when anomaly detections is allowed and when it is not, across various anomaly conditions and ten data generating seeds.

of the system. Thus, we end up with the number of people entering a station every operating hour of every station.

Such data can be represented as a three-dimensional tensor. The first mode of the tensor represents the stations, while the second and third modes represent the day and the time of day, respectively. Thus, we expect to obtain clusters at the station level using the clustering objective and point anomalies at hourly resolution.

Understanding commonalities between stations is important from an urban mobility perspective. The stations that are similar to each other in terms of passenger inflow may reveal what kind of features about those stations are the most influential in people's decision to take the subway on a specific day and time of day.

Detecting anomalies is also important from a managerial point of view. Generally, urban mobility shows strong predictability due to the regular weekly schedules of city dwellers. However, rare events could occur,

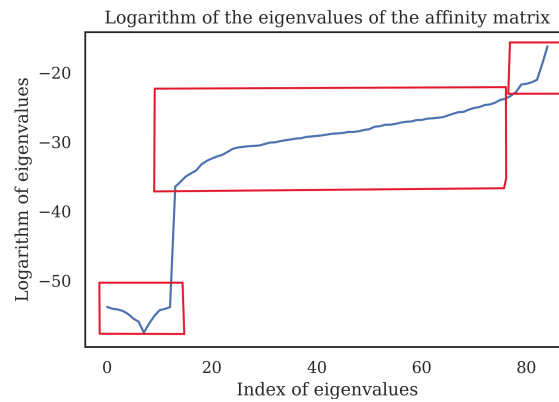


Figure 7 Eigenvalue spectrum of the affinity matrix to locate discontinuous segments

and the subway management would rather take precautions in the face of such events. Detection of past point anomalies may reveal the underlying reasons for one-off events that lead to extreme passenger inflow, such as concerts, celebrations, or extreme weather events. Armed with this knowledge, subway management can be more accurate in predicting future rare events.

5.1. Station Clustering

We trained our model with the smart card data and recovered three clusters. The number of clusters was determined using the method introduced in Von Luxburg (2007). We first plot the logarithm of the eigenvalue spectrum of the Laplacian of the affinity matrix, then locate the discontinuous segments, as shown in Figure 7.

Figure 8 and Figure 9, when observed jointly, reveal important insight into how the stations are clustered. Weekdays play the primary role in determining the cluster of a station. As shown in the Figure 8, the first cluster (Cluster ID: 0, colored in green) has a strong inflow peak at the morning peak hour. These stations are also mainly located in the residential areas of Hong Kong (i.e., west and east end of Hong Kong Island, west side of New Territories, east side of Kowloon), as shown in the Figure 9, Likewise, for the second cluster (Cluster ID: 1, colored in orange), we observe a strong evening peak inflow as opposed to the mornings, and they are mostly located in the business region such as the Central area of Hong Kong Island and the opposite side in Kowloon, as shown in Figure 9. As we could conclude so far, for the most part, this can be explained by the land use, specifically, whether it is residential or work and office space. The third cluster (Cluster ID: 2, colored in purple) does not have a dominant peak between the morning and evening, and the rest of the inflow is rather evenly distributed throughout the day. While not as prominent as weekdays, weekends (especially Saturday) patterns also differ from one cluster to another.

Interpretation of the third cluster requires some contextual investigation. Hong Kong draws millions of visitors each year, especially from the bordering Shenzhen City, Guangdong Province of mainland China. The third cluster is a collection of stations where visitors enter Hong Kong, with the primary intention being

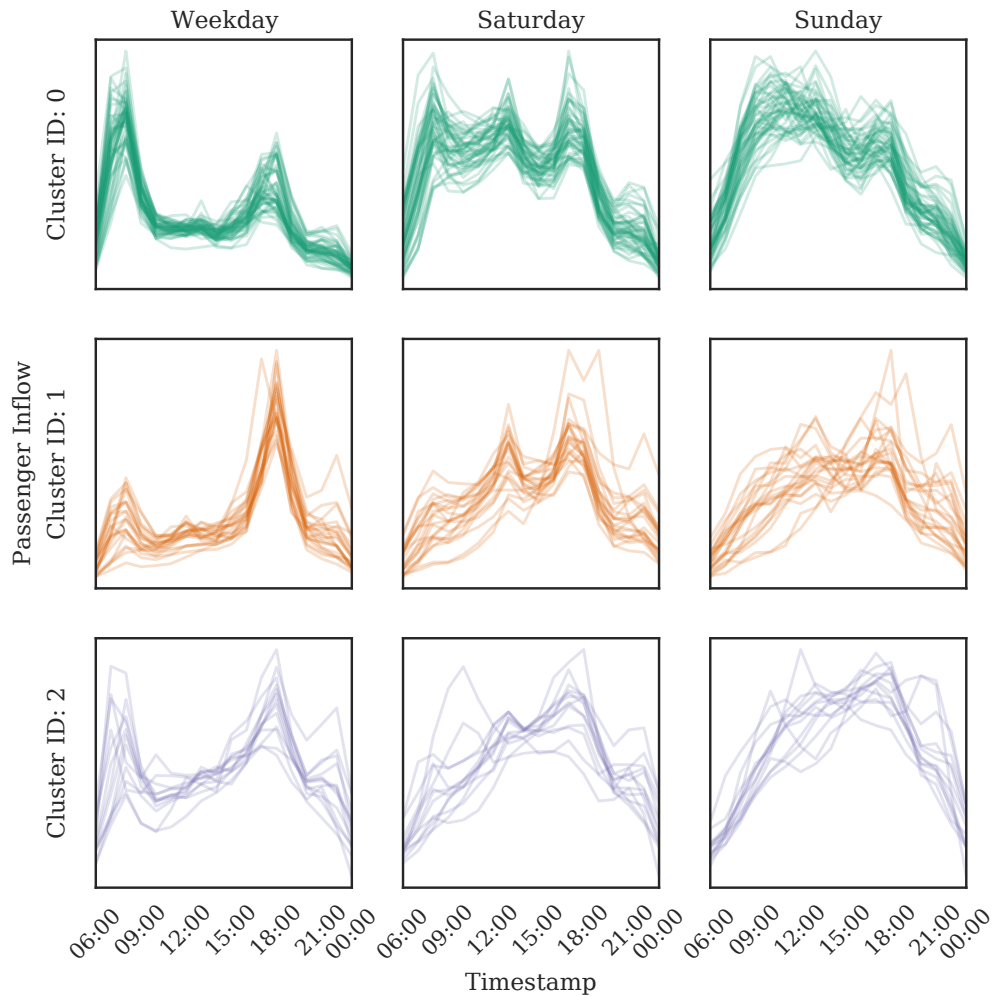


Figure 8 Hourly inflow patterns per cluster on a randomly picked week, across weekdays and weekend days. The color coding matches with the stations in Figure 9.

cross-border shopping. The absence of taxes and duties on goods in Hong Kong makes it an appealing destination for Chinese visitors to shop. Since shopping is not a strictly time-bound activity, we observe inflows that are dispersed more homogeneously around the day, both on weekdays and weekends.

We now bring in the land use information¹ to the picture. In Figure 10, the first and second clusters can strictly be separated by the prevalence of residential areas or commercial and industrial areas, respectively. The only station from the third cluster, Sha Tin station, is surrounded by many shopping malls, with an iconic *New Town Plaza* which offers around 2 million sq. ft. of exceptional more than 400 shopping, dining,

¹Open data via https://www.pland.gov.hk/pland_en/info_serv/open_data/landu/index.html

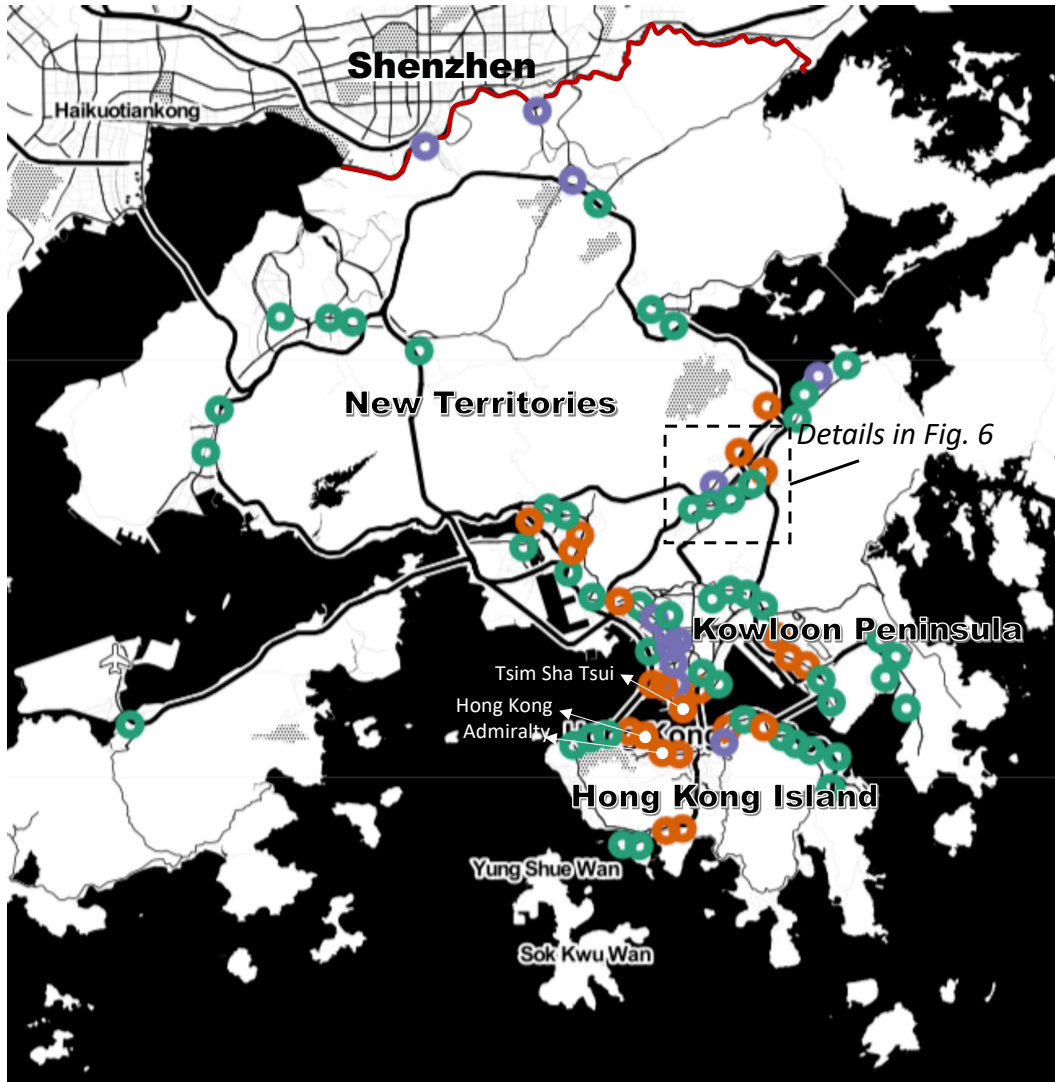


Figure 9 Hong Kong subway stations on a map, clustered three-way. Colors represent different clusters. Circle radius represents a typical walking distance of 400 meters around the station.

and lifestyle facilities. Thus, it is a popular shopping destination for passengers visiting from mainland China.

We can analyze even more thoroughly with granular information. The key takeaway is that the clustering of stations yields important insight into the factors that determine passenger inflows.

5.2. Detected Point Anomalies

We now focus on the point anomalies detected by the proposed model in the data from the smart card. As we have discussed before, one-off events are an important determinant of irregular patterns in passenger inflows.

Lunar New Year celebrations in Hong Kong, which took place between 28th and 31st of January in Victoria Harbor between Hong Kong Island and the Kowloon Peninsula, yield a number of other rare events. One

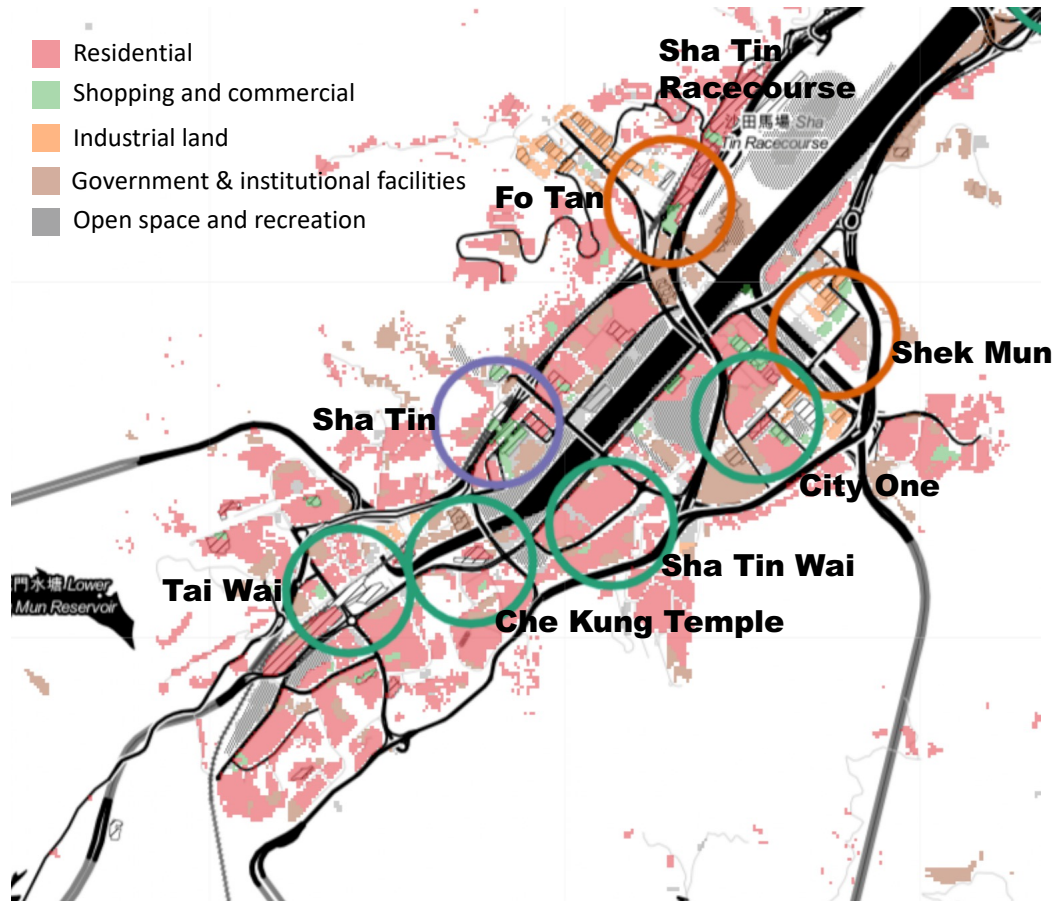


Figure 10 Sha Tin and Tai Wai regions with land use information. The circle color coding of clusters matches with the stations in Figure 9. The land use color coding logic is as follows: Red: residential, Green: commercial, Orange: industrial, Brown: institutional, governmental, and Grey: parks and recreations.

of the events is the Lunar New Year Fireworks Display. In Figure 11, we observe the peaks related to that event in the Tsim Sha Tsui station, Admiralty and Hong Kong, with locations pinned in Figure 9. These stations are close to places that are considered the best places to watch the fireworks display.

Another interesting rare event takes place at the Hung Hom station. In Figure 11, we observed an unusual peak at 8 pm for four consecutive days from February 16th to February 19th. This suggests the scheduled end of a four-day event, perhaps a conference, given the proximity of the station to Hong Kong Polytechnic University.

In general, detected anomalies are promising in terms of the amount of insight they can provide for public transportation management.

6. Conclusion

In this paper, we focused on the problem of spatio-temporal modeling with tensors. Specifically, we proposed a tensor decomposition-based model that is capable of simultaneous clustering and point anomaly detection, all of which are important challenges to be addressed in this kind of data. Our simulation study

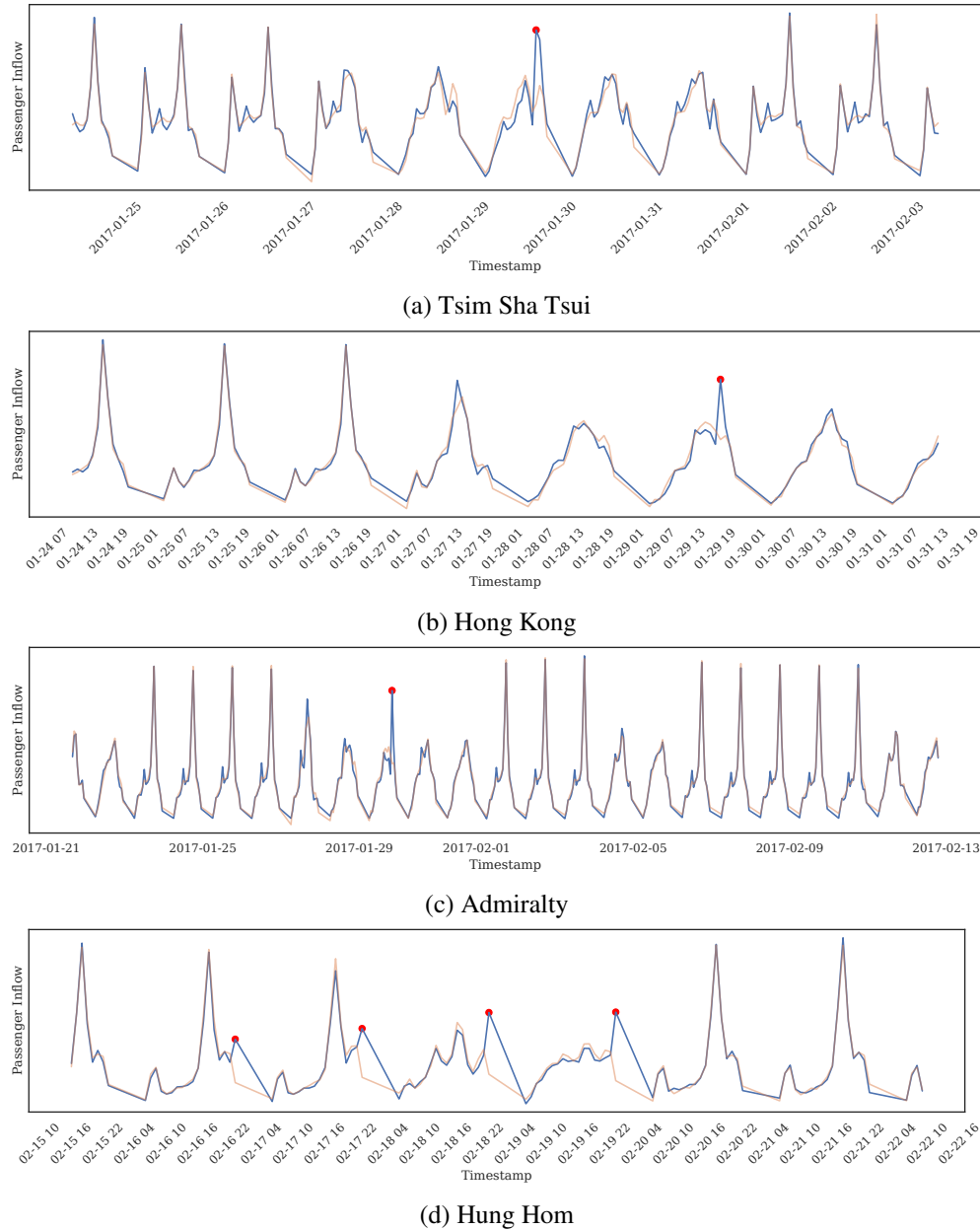


Figure 11 Examples of rare events in five different stations, detected as point anomalies over passenger inflows.

shows that, in general, point anomaly detection increases clustering accuracy when point anomalies exist in data and vice versa. As for the case study, we trained our model on a collection of smart card transactions from the subway system of Hong Kong. Our model was able to effectively recover station clusters that are semantically consistent both temporally and spatially. The model was also able to recover rare events in terms of point anomalies, which offers valuable insights and assistance for managerial analysis and operations.

Appendix A: Appendix

A.1. Proof of Proposition 3.1

We rearrange the objective functions as follows:

$$\begin{aligned}
\mathcal{L}_{\mathbf{Z}} &\triangleq \frac{1}{2} \|\mathbf{Z}\|_F^2 + \frac{\lambda_z}{2} \|\mathbf{C}_{(1)} - \mathbf{Z}\mathbf{C}_{(1)}\|_F^2 \\
&= \frac{1}{2} \text{tr}(\mathbf{Z}^\top \mathbf{Z}) + \frac{\lambda_z}{2} \text{tr}(\mathbf{C}_{(1)}^\top \mathbf{C}_{(1)} - 2\mathbf{C}_{(1)}^\top \mathbf{Z}\mathbf{C}_{(1)} + \mathbf{C}_{(1)}^\top \mathbf{Z}^\top \mathbf{Z}\mathbf{C}_{(1)}) \\
&= \frac{1}{2} \text{tr}(\mathbf{Z}^\top \mathbf{Z}) + \frac{\lambda_z}{2} (\text{tr}(\mathbf{C}_{(1)}^\top \mathbf{C}_{(1)}) - 2\text{tr}(\mathbf{C}_{(1)}^\top \mathbf{Z}\mathbf{C}_{(1)}) + \text{tr}(\mathbf{C}_{(1)}^\top \mathbf{Z}^\top \mathbf{Z}\mathbf{C}_{(1)})) \\
&= \frac{1}{2} \text{tr}(\mathbf{Z}^\top \mathbf{Z}) + \frac{\lambda_z}{2} (\text{tr}(\mathbf{C}_{(1)}^\top \mathbf{C}_{(1)}) - 2\text{tr}(\mathbf{C}_{(1)}^\top \mathbf{Z}\mathbf{C}_{(1)}) + \text{tr}(\mathbf{C}_{(1)} \mathbf{C}_{(1)}^\top \mathbf{Z}^\top \mathbf{Z}))
\end{aligned}$$

Taking the derivative of $\mathcal{L}_{\mathbf{Z}}$ with respect to \mathbf{Z} we get:

$$\frac{\partial \mathcal{L}_{\mathbf{Z}}}{\partial \mathbf{Z}} = \mathbf{Z} - \lambda_z (\mathbf{C}_{(1)} \mathbf{C}_{(1)}^\top) + \lambda_z \mathbf{C}_{(1)} \mathbf{C}_{(1)}^\top \mathbf{Z}$$

Setting $\frac{\partial \mathcal{L}_{\mathbf{Z}}}{\partial \mathbf{Z}} = \mathbf{0}$, we find the closed-form solution \mathbf{Z}^* as in Equation (6).

A.2. Proof of Proposition 3.3

Rearranging the terms, we get the following objective function:

$$\begin{aligned}
\mathcal{L}_{\mathbf{C}_{(1)}} &\triangleq \frac{\lambda_z}{2} \|\mathbf{C}_{(1)} - \mathbf{Z}\mathbf{C}_{(1)}\|_F^2 + \frac{\lambda_e}{2} \|\mathbf{M} - \mathbf{C}_{(1)}\mathbf{P}\|_F^2 \\
&= \frac{\lambda_z}{2} \text{tr}(\mathbf{C}_{(1)}^\top (\mathbf{I} - \mathbf{Z})^\top (\mathbf{I} - \mathbf{Z}) \mathbf{C}_{(1)}) + \\
&\quad \frac{\lambda_e}{2} \text{tr}(\mathbf{M}^\top \mathbf{M} - 2\mathbf{M}^\top \mathbf{C}_{(1)}\mathbf{P} + \mathbf{P}^\top \mathbf{C}_{(1)}^\top \mathbf{C}_{(1)}\mathbf{P}) \\
&= \frac{\lambda_z}{2} \text{tr}(\mathbf{C}_{(1)}^\top (\mathbf{I} - \mathbf{Z})^\top (\mathbf{I} - \mathbf{Z}) \mathbf{C}_{(1)}) + \frac{\lambda_e}{2} \text{tr}(\mathbf{M}^\top \mathbf{M}) \\
&\quad - \lambda_e \text{tr}(\mathbf{P}\mathbf{M}^\top \mathbf{C}_{(1)}) + \frac{\lambda_e}{2} \text{tr}(\mathbf{P}\mathbf{P}^\top \mathbf{C}_{(1)}^\top \mathbf{C}_{(1)})
\end{aligned}$$

Taking the derivative of $\mathcal{L}_{\mathbf{C}_{(1)}}$ with respect to $\mathbf{C}_{(1)}$ we get:

$$\frac{\partial \mathcal{L}_{\mathbf{C}_{(1)}}}{\partial \mathbf{C}_{(1)}} = \lambda_z (\mathbf{I} - \mathbf{Z})^\top (\mathbf{I} - \mathbf{Z}) \mathbf{C}_{(1)} - \lambda_e \mathbf{M}\mathbf{P}^\top + \lambda_e \mathbf{P}\mathbf{P}^\top \mathbf{C}_{(1)}$$

Here, notice that $\mathbf{P}\mathbf{P}^\top = (\mathbf{U}_3^\top \otimes \mathbf{U}_2^\top)(\mathbf{U}_3 \otimes \mathbf{U}_2) = (\mathbf{U}_3^\top \mathbf{U}_3) \otimes (\mathbf{U}_2^\top \mathbf{U}_2) = \mathbf{I}$, because of the properties of the Kronecker product and \mathbf{U}_2 and \mathbf{U}_3 being orthonormal matrices. This helps us simplify the closed-form solution $\mathbf{C}_{(1)}^*$ which is found by setting $\frac{\partial \mathcal{L}_{\mathbf{C}_{(1)}}}{\partial \mathbf{C}_{(1)}} = \mathbf{0}$.

A.3. Proof of Proposition 3.4

By unfolding the tensor into the 2nd mode, we have

$$\begin{aligned}
&\arg \min_{\mathbf{U}_2} \frac{\lambda_e}{2} \|\mathcal{X} - \mathcal{A} - \mathcal{C} \times_2 \mathbf{U}_2 \times_3 \mathbf{U}_3\|_F^2 \\
&= \arg \min_{\mathbf{U}_2} \|\mathbf{X}_{(2)} - \mathbf{A}_{(2)} - \mathbf{U}_2 \mathbf{C}_{(2)} (\mathbf{U}_3 \otimes \mathbf{I})^\top\|_F^2 \\
&= \arg \min_{\mathbf{U}_2} \|\mathbf{B}_1 - \mathbf{U}_2 \mathbf{B}_2\|_F^2,
\end{aligned}$$

where $\mathbf{B}_1 = \mathbf{X}_{(2)} - \mathbf{A}_{(2)}$ and $\mathbf{B}_2 = \mathbf{C}_{(2)}(\mathbf{U}_3 \otimes \mathbf{I})^T$. In this form, this problem has the same structure as the orthogonal Procrustes problem (Schönemann 1966).

The solution is given by the SVD decomposition on $\mathbf{Q} = \mathbf{B}_1 \mathbf{B}_2^T = (\mathbf{X}_{(2)} - \mathbf{A}_{(2)})(\mathbf{U}_3 \otimes \mathbf{I})\mathbf{C}_{(2)}^T$ as $\mathbf{Q} = \hat{\mathbf{U}}\mathbf{D}\hat{\mathbf{V}}^T$. Finally, the solution is $\mathbf{U}_2^* = \hat{\mathbf{U}}\hat{\mathbf{V}}^T$.

Acknowledgments

This work is partially funded by the Hong Kong Research Grants Council (RGC) under the grants RGC GRF 16201718 and 16216119.

References

- Aggarwal CC (2015) Outlier analysis. *Data mining*, 237–263 (Springer).
- Bahadori MT, Yu QR, Liu Y (2014) Fast multivariate spatio-temporal analysis via low rank tensor learning. *Advances in neural information processing systems*, 3491–3499.
- Chandola V, Banerjee A, Kumar V (2009) Anomaly detection: A survey. *ACM computing surveys (CSUR)* 41(3):1–58.
- Drakopoulos G, Spyrou E, Mylonas P (2019) Tensor clustering: A review. *2019 14th International Workshop on Semantic and Social Media Adaptation and Personalization (SMAP)*, 1–6 (IEEE).
- Du B, Zhang L (2014) A discriminative metric learning based anomaly detection method. *IEEE Transactions on Geoscience and Remote Sensing* 52(11):6844–6857.
- Fanaee-T H, Gama J (2016) Tensor-based anomaly detection: An interdisciplinary survey. *Knowledge-Based Systems* 98:130–147.
- Fu Y, Gao J, Tien D, Lin Z (2014) Tensor lrr based subspace clustering. *2014 International Joint Conference on Neural Networks (IJCNN)*, 1877–1884 (IEEE).
- Fu Y, Gao J, Tien D, Lin Z, Hong X (2016) Tensor lrr and sparse coding-based subspace clustering. *IEEE transactions on neural networks and learning systems* 27(10):2120–2133.
- Gahrooei MR, Yan H, Paynabar K, Shi J (2021) Multiple tensor-on-tensor regression: An approach for modeling processes with heterogeneous sources of data. *Technometrics* 63(2):147–159.
- Gao H, Nie F, Li X, Huang H (2015) Multi-view subspace clustering. *Proceedings of the IEEE international conference on computer vision*, 4238–4246.
- Guo K, Zhang T, Xu X, Xing X (2019) Low-rank tensor thresholding ridge regression. *IEEE Access* 7:153761–153772.
- He Y, Atia GK (2022) Multi-mode tensor space clustering based on low-tensor-rank representation. *Proceedings of the AAAI Conference on Artificial Intelligence*, volume 36, 6893–6901.
- Heng Q, Chi EC, Liu Y (2023) Robust low-rank tensor decomposition with the l2 criterion. *Technometrics* 65(4):537–552.
- Hitchcock FL (1927) The expression of a tensor or a polyadic as a sum of products. *Journal of Mathematics and Physics* 6(1-4):164–189.

- Hu Y, Work DB (2021) Robust tensor recovery with fiber outliers for traffic events. *ACM Trans. Knowl. Discov. Data* 15(1), ISSN 1556-4681.
- Huang H, Ding C, Luo D, Li T (2008) Simultaneous tensor subspace selection and clustering: the equivalence of high order svd and k-means clustering. *Proceedings of the 14th ACM SIGKDD international conference on Knowledge Discovery and Data mining*, 327–335.
- Huang S, Zhang H, Zeng H, Pižurica A (2023) From model-based optimization algorithms to deep learning models for clustering hyperspectral images. *Remote Sensing* 15(11):2832.
- Jegelka S, Sra S, Banerjee A (2009) Approximation algorithms for tensor clustering. *International Conference on Algorithmic Learning Theory*, 368–383 (Springer).
- Kolda TG, Bader BW (2009) Tensor decompositions and applications. *SIAM review* 51(3):455–500.
- Li Z (2021) Tensor topic models with graphs and applications on individualized travel patterns. *2021 IEEE 37th International Conference on Data Engineering (ICDE)*, 2756–2761 (IEEE).
- Li Z, Sergin ND, Yan H, Zhang C, Tsung F (2020a) Tensor completion for weakly-dependent data on graph for metro passenger flow prediction. *proceedings of the AAAI conference on artificial intelligence*, volume 34, 4804–4810.
- Li Z, Yan H, Tsung F, Zhang K (2022a) Profile decomposition based hybrid transfer learning for cold-start data anomaly detection. *ACM Transactions on Knowledge Discovery from Data (TKDD)* .
- Li Z, Yan H, Zhang C, Tsung F (2020b) Long-short term spatiotemporal tensor prediction for passenger flow profile. *IEEE Robotics and Automation Letters* 5(4):5010–5017.
- Li Z, Yan H, Zhang C, Tsung F (2022b) Individualized passenger travel pattern multi-clustering based on graph regularized tensor latent dirichlet allocation. *Data Mining and Knowledge Discovery* 1–32.
- Lin C, Zhu Q, Guo S, Jin Z, Lin YR, Cao N (2018) Anomaly detection in spatiotemporal data via regularized non-negative tensor analysis. *Data Mining and Knowledge Discovery* 32(4):1056–1073.
- Liu G, Lin Z, Yan S, Sun J, Yu Y, Ma Y (2013) Robust recovery of subspace structures by low-rank representation. *IEEE Trans. Pattern Anal. Mach. Intell.* 35(1):171–184.
- Liu G, Zhang Z, Liu Q, Xiong H (2019) Robust subspace clustering with compressed data. *IEEE Transactions on Image Processing* 28(10):5161–5170.
- Lock EF (2018) Tensor-on-tensor regression. *Journal of Computational and Graphical Statistics* 27(3):638–647.
- Lu H, Plataniotis KN, Venetsanopoulos AN (2008a) MPCA: Multilinear principal component analysis of tensor objects. *IEEE transactions on Neural Networks* 19(1):18–39.
- Lu H, Plataniotis KN, Venetsanopoulos AN (2008b) Uncorrelated multilinear principal component analysis through successive variance maximization. *Proceedings of the 25th international conference on Machine learning*, 616–623.
- Mao Z, Li Z, Li D, Bai L, Zhao R (2022) Jointly contrastive representation learning on road network and trajectory. *arXiv preprint arXiv:2209.06389* .

- Nomikos P, MacGregor JF (1994) Monitoring batch processes using multiway principal component analysis. *AIChE Journal* 40(8):1361–1375.
- Pan SJ, Yang Q (2009) A survey on transfer learning. *IEEE Transactions on knowledge and data engineering* 22(10):1345–1359.
- Parsons L, Haque E, Liu H (2004) Subspace clustering for high dimensional data: a review. *Acm sigkdd explorations newsletter* 6(1):90–105.
- Pelletier MP, Trépanier M, Morency C (2011) Smart card data use in public transit: A literature review. *Transportation Research Part C: Emerging Technologies* 19(4):557–568.
- Peng X, Yi Z, Tang H (2015) Robust subspace clustering via thresholding ridge regression. *Proceedings of the AAAI Conference on Artificial Intelligence*, volume 29.
- Shen B, Xie W, Kong ZJ (2022) Smooth robust tensor completion for background/foreground separation with missing pixels: Novel algorithm with convergence guarantee. *Journal of Machine Learning Research* 23(217):1–40.
- Sofuoglu SE, Aviyente S (2021) Low-rank on graphs plus temporally smooth sparse decomposition for anomaly detection in spatiotemporal data. *ICASSP 2021-2021 IEEE International Conference on Acoustics, Speech and Signal Processing (ICASSP)*, 5614–5618 (IEEE).
- Sun B, Zhao Z, Liu D, Gao X, Yu T (2022) Tensor decomposition-inspired convolutional autoencoders for hyperspectral anomaly detection. *IEEE Journal of Selected Topics in Applied Earth Observations and Remote Sensing* 15:4990–5000.
- Sun WW, Li L (2019) Dynamic tensor clustering. *Journal of the American Statistical Association* 114(528):1894–1907.
- Tucker LR (1966) Some mathematical notes on three-mode factor analysis. *Psychometrika* 31(3):279–311.
- Vidal R (2011) Subspace clustering. *IEEE Signal Process. Mag.* 28(2):52–68.
- Vidal R, Favaro P (2014) Low rank subspace clustering (LRSC). *Pattern Recognit. Lett.* 43:47–61.
- Vidal R, Tron R, Hartley R (2008) Multiframe motion segmentation with missing data using powerfactorization and gpca. *International Journal of Computer Vision* 79(1):85–105.
- von Luxburg U (2007) A tutorial on spectral clustering. *Stat. Comput.* 17(4):395–416.
- Von Luxburg U (2007) A tutorial on spectral clustering. *Statistics and computing* 17:395–416.
- Wang M, Zhen Y, Pan Y, Xu Z, Guo R, Zhao X (2023) Tensorized hypergraph neural networks. *arXiv preprint arXiv:2306.02560* .
- Xue N, Papamakarios G, Bahri M, Panagakis Y, Zafeiriou S (2017) Robust low-rank tensor modelling using tucker and cp decomposition. *2017 25th European Signal Processing Conference (EUSIPCO)*, 1185–1189 (IEEE).
- Yan H, Paynabar K, Shi J (2015) Image-Based process monitoring using Low-Rank tensor decomposition. *IEEE Trans. Autom. Sci. Eng.* 12(1):216–227.

- Yan H, Paynabar K, Shi J (2017) Anomaly detection in images with smooth background via smooth-sparse decomposition. *Technometrics* 59(1):102–114.
- Yan H, Paynabar K, Shi J (2018) Real-Time monitoring of High-Dimensional functional data streams via Spatio-Temporal smooth sparse decomposition. *Technometrics* 60(2):181–197.
- Yang C, Robinson D, Vidal R (2015) Sparse subspace clustering with missing entries. *International Conference on Machine Learning*, 2463–2472.
- Yang S, Wu J, Xu Y, Yang T (2019) Revealing heterogeneous spatiotemporal traffic flow patterns of urban road network via tensor decomposition-based clustering approach. *Physica A: Statistical Mechanics and its Applications* 526:120688, ISSN 0378-4371.
- Zhang C, Fu H, Liu S, Liu G, Cao X (2015) Low-rank tensor constrained multiview subspace clustering. *Proceedings of the IEEE international conference on computer vision*, 1582–1590.
- Zhang C, Yan H, Lee S, Shi J (2020) Dynamic multivariate functional data modeling via sparse subspace learning. *Technometrics* 1–14.
- Zhang C, Zheng B, Tsung F (2023) Multi-view metro station clustering based on passenger flows: a functional data-edged network community detection approach. *Data Mining and Knowledge Discovery* 37(3):1154–1208.
- Zhao X, Dai Q, Wu J, Peng H, Liu M, Bai X, Tan J, Wang S, Philip SY (2022a) Multi-view tensor graph neural networks through reinforced aggregation. *IEEE Transactions on Knowledge and Data Engineering* 35(4):4077–4091.
- Zhao X, Yan H, Hu Z, Du D (2022b) Deep spatio-temporal sparse decomposition for trend prediction and anomaly detection in cardiac electrical conduction. *IIEE Transactions on Healthcare Systems Engineering* 12(2):150–164.
- Zhao Y, Yan H, Holte S, Mei Y (2021) Rapid detection of hot-spots via tensor decomposition with applications to crime rate data. *Journal of Applied Statistics* 1–27.
- Zhao Y, Yan H, Holte SE, Kerani RP, Mei Y (2020) Rapid detection of hot-spot by tensor decomposition on space and circular time with application to weekly gonorrhoea data. *THE XIIIITH INTERNATIONAL WORKSHOP ON INTELLIGENT STATISTICAL QUALITY CONTROL 2019*.